Supplementary material for the manuscript "Bonferroni Mean Pre-aggregation Operator Assisted Dynamic Fuzzy Histogram Equalization for Retinal Vascular Segmentation"

Purpose of the survey (A survey on the analysis of disease prediction and changes in the structure of vessels in the fundus and OCT images)

- Identification of retinal diseases through fundus image analysis.
- The featured image of the fundus images does assist in characterizing the disease identification more robustly.
- Study the inter-relation and relative efficiency of multi-modality Fundus and OCT image utilization.
- **Link:**https://docs.google.com/forms/d/e/1FAIpQLSdBKW4J4EaawK0LwJZhoPIIh6S9NasoBSqFcHMzXGh4qDurdg/viewform?usp=pp_url

Theortical Propositions and Proofs

Proposition 1.1: For an eligible function C^* such that it is left conjunctive, and an eligible function M_2^*, the operator $B_{M_2^*}^{C^*}$ fulfills the boundary condition at the extreme point $\vec{0}$.

Proof 1.1: Since, C^* is left conjunctive, so we have $C^*(x,y) \leq x$, $\forall\ x,y \in [0,1]$, which implies $C^*(0,y) = 0$, $\forall\ y \in [0,1]$. Consider,

$$B_{M_2^*}^{C^*}(0,...,0) = \delta_{C^*}^{-1}\left[\frac{1}{n}\sum_{i=1}^{n} C^*(0, M_2^*(0 : j = 1\ to\ n,\ j \neq i))\right]$$
$$= \delta_{C^*}^{-1}\{0\}$$

The injectivity of the function δ_{C^*} implies that $C^*(0,0) = 0 = \delta_{C^*}(0)$, so we have

$$B_{M_2^*}^{C^*}(0,...,0) = \delta_{C^*}^{-1}\{\delta_{C^*}(0)\} = 0.$$

Hence, the boundary condition is satisfied at the extreme point $\vec{0}$.

Remark 1.1: It is to be noted that the function M_2^* may not satisfy the boundary condition at the extreme point $\vec{0}$. For instance, on taking $n = 2$, let $M_2^*(x) = 1 - x$, $\forall\ x \in [0,1]$, then M_2^* does not satisfy the boundary conditions. But, if one takes C^* as a left conjunctive operator, then the boundary condition at the extreme point $\vec{0}$ is satisfied by the operator $B_{M_2^*}^{C^*}$, irrespective of the operator M_2^*.

Proposition 1.2: The sufficient condition for the operator $B_{M_2^*}^{C^*}$ to satisfy the boundary condition at the extreme point $\vec{1}$ is that the eligible function M_2^* is idempotent.

Proof 1.2: It is easy to verify that if the eligible function M_2^* is idempotent, then $B_{M_2^*}^{C^*}$ satisfies boundary condition at $\vec{1}$.

Proposition 1.3: For any eligible function $C^* : [0,1]^2 \mapsto [0,1]$ such that C^* is $(1,1)$-increasing, and for any eligible function M_2^* such that it is $\vec{1}$-increasing, the operator $B_{M_2^*}^{C^*}$ is a $\vec{1}$-increasing operator.

Proof 1.3: First, we prove that if C^* is $(1,1)$-increasing function, then δ_{C^*} is a non-decreasing function. For this, let $c > 0$, and consider,

$$\delta_{C^*}(x+c) = C^*(x+c, x+c) \geq C^*(x,x) = \delta_{C^*}(x)\ \forall\ x \in [0,1].$$

Hence, δ_{C^*} is a non-decreasing operator. Due to bijection of the operator δ_{C^*}, we have δ_{C^*}, and hence the function $\delta_{C^*}^{-1}$ as a strictly increasing function.

To show that $B_{M_2^*}^{C^*}$ is $\vec{1}$-increasing operator, let $(x_1,...,x_n) \in [0,1]^n$, and consider

$$B_{M_2^*}^{C^*}(x_1+c,...,x_n+c) = \delta_{C^*}^{-1}\Bigg[\frac{1}{n}\sum_{i=1}^{n} C^*(x_i+c, M_2^*(x_j+c$$
$$: j = 1\ to\ n,\ j \neq i))\Bigg].$$

Since, M_2^* is $\vec{1}$-increasing, so we have,

$$M_2^*(x_j+c : j = 1\ to\ n,\ j \neq i) \geq M_2^*(x_j : j = 1\ to\ n,\ j \neq i).$$

Also, C^* is an aggregation function, so we have,

$$C^*(x_i+c, M_2^*(x_j+c : j = 1\ to\ n,\ j \neq i)) \geq C^*(x_i, M_2^*(x_j :$$
$$j = 1\ to\ n,\ j \neq i))$$
$$\Rightarrow \sum_{i=1}^{n}\Big\{C^*(x_i+c, M_2^*(x_j+c : j = 1\ to\ n,\ j \neq i))\Big\}$$
$$\geq \sum_{i=1}^{n}\Big\{C^*(x_i, M_2^*(x_j : j = 1\ to\ n,\ j \neq i))\Big\}$$

Due to strictly increasingness of the function $\delta_{C^*}^{-1}$ over $[0,1]$, the proof of the proposition follows.

To construct the pre-aggregation function the following conditions should satisfy which is obtain by combining the aforementioned statements and it is described as follows:

Corollary 1.1: Let the eligible functions C^* and M_2^* satisfies the following properties:

1) C^* is left conjunctive and $(1,1)$-increasing function;
2) M_2^* is idempotent and $\vec{1}$-increasing;

then the corresponding $B_{M_2^*}^{C^*}$ is a pre-aggregation function.

AGGREGATION OPERATOR FOR BENCHMARK

The proposed Bonferroni mean pre-aggregation operator is defined as:

$$B^{C^*}_{M_2^*}(\mathbf{x}) = \delta^{-1}_{C^*}\left[\frac{1}{n}\sum_{i=1}^{n} C^*(x_i, M_2^*(x_j : j = 1 \quad to \quad n, j \neq i))\right] \tag{1S}$$

where $\mathbf{x} = (x_1, ..., x_n) \in [0, 1]^n$.

We have considered three different forms of C^* and M_2^* in Eq. 1S, and obtain the Bonferroni mean pre-aggregation operator and Bonferroni mean aggregation operator as presented in Table 1S. Additionally, we have considered the often-used classical aggregation operator Maximum and Averaging presented in Table 1S. The quantitative analysis is conducted using the presented operators in the BMPDFHESeg method over the DRIVE, STARE, and HRF datasets. The experimental results are reported in Table 2S. The quantitative performance of F_3 is better compared to the other operators used in the BMPDFHESeg method.

VISUAL COMPARISON BETWEEN THE L_1, L_2, AND L_∞ NORMS

We have extracted the feature maps by taking a sample image from the DRIVE dataset and employed L_1, L_2, and L_∞ norms during the feature extraction process and outcomes are shown in Fig. 1S. The inserts show a zoomed appearance of vasculature features as shown in Fig. 1S. It can be noted from Fig. 1S (a) that the L_1 norm can preserve the strong gradient while extraction of vascular features compared to L_2 and L_∞ norm. Whereas the L_2 norm tries to smooth out the feature information and is sensitive to the outliers, leading to loss of the vascular feature information. The performance of L_∞ norm is more sensitive and not able to preserve the strong gradient information, as shown in Fig. 1S (c). Therefore, the performance of L_1 norm is more reliable compared to L_2 and L_∞.

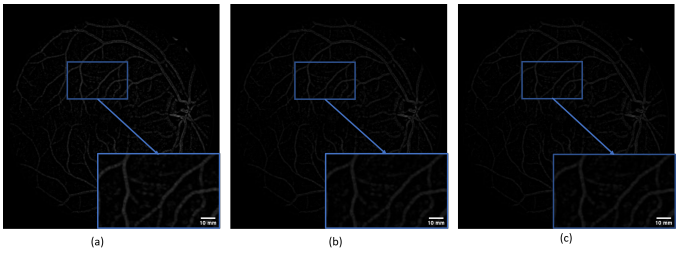

Fig. 1S. Analysis of feature map generated through (a) L_1, (b) L_2, and (c) L_∞ norms utilized in the BMPDFHESeg method.

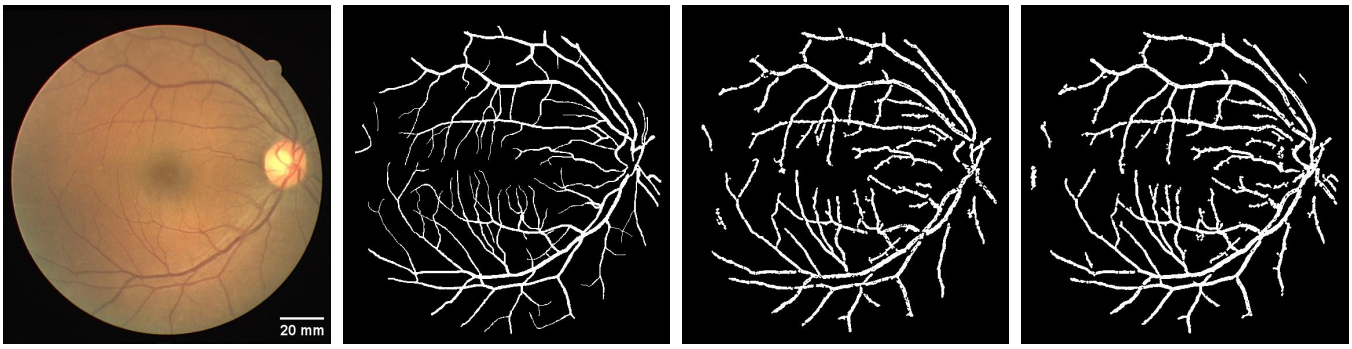

Fig. 2S. Sample image from DRIVE dataset (a) original fundus image, (b) ground truth image, (c) segmentation results of green channel response, and (d) segmentation results of color fusion response.

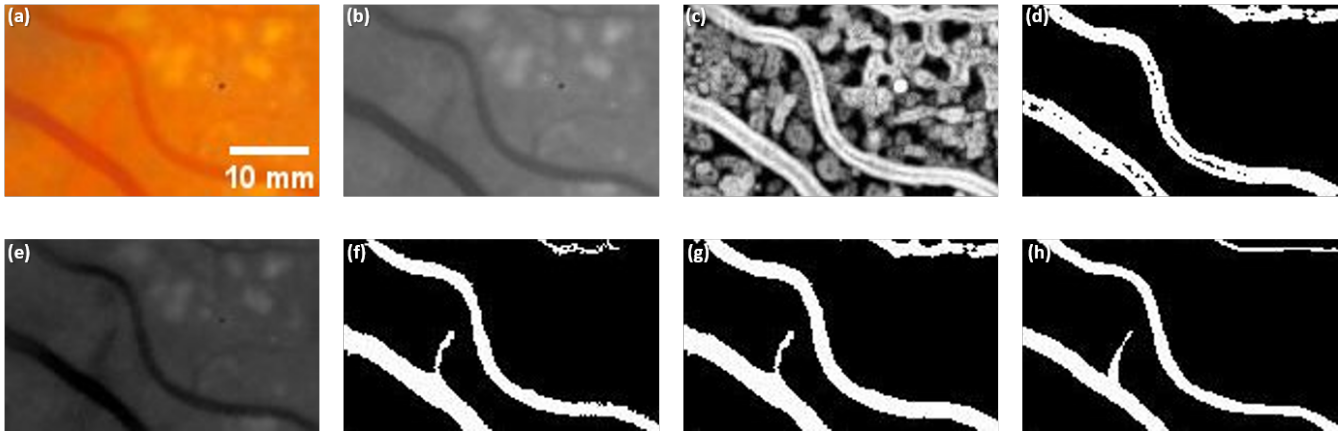

Fig. 3S. (a) Enlarged region of an image from STARE dataset, (b) green channel region, (c) vessel's feature extraction region, (d) prominent feature map region, (e) enhanced green channel region through fuzzy histogram equalization technique by using vessel's feature gray levels, (f) segmented vessels region of the enhanced green channel, (g) final segmented enhanced vessel region, and (h) ground truth enlarged region.

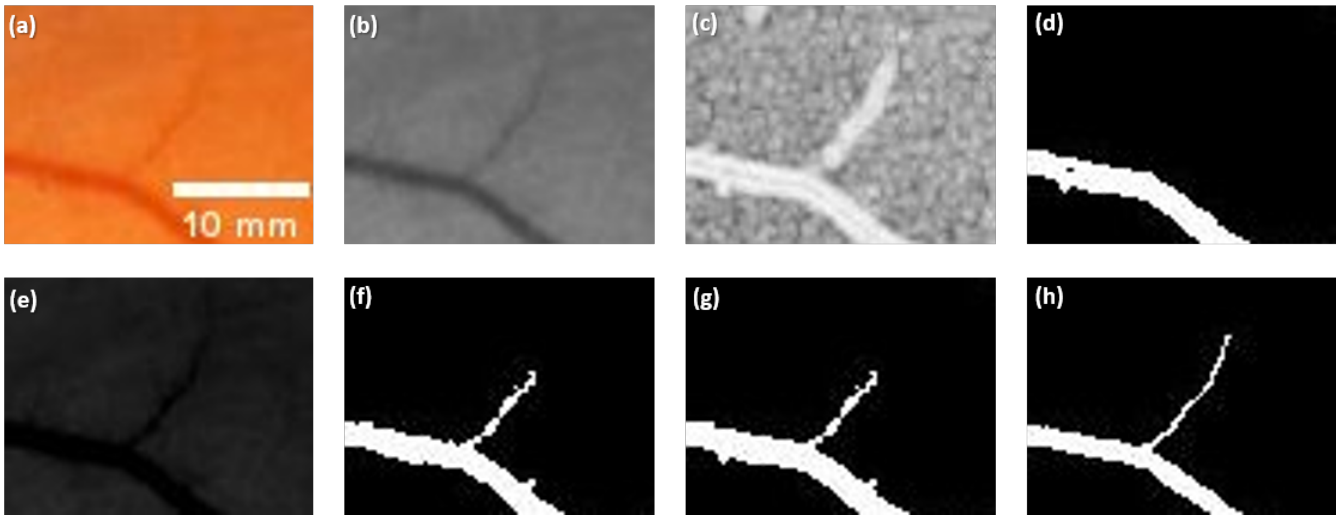

Fig. 4S. (a) Enlarged region of an image from STARE dataset, (b) green channel region, (c) vessel's feature extraction region, (d) prominent feature map region, (e) enhanced green channel region through fuzzy histogram equalization technique by using vessel's feature gray levels, (f) segmented vessels region of the enhanced green channel, (g) final segmented enhanced vessel region, and (h) ground truth enlarged region.

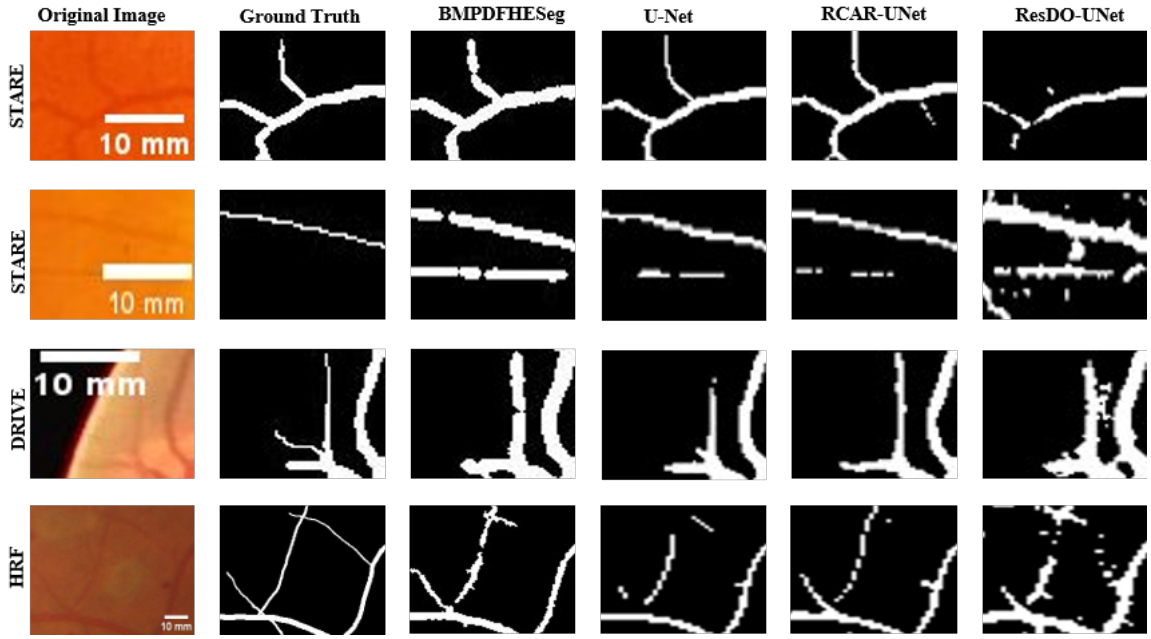

Fig. 5S. Enlarged region of images from DRIVE, STARE, and HRF datasets obtained through the BMPDFHESeg method compared with U-Net [1], RCAR-UNet [2], and ResDO-UNet [3] models.

Table 1S
CONSIDERED BONFERRONI MEAN PRE-AGGREGATION OPERATOR AND AGGREGATION OPERATOR FOR BENCHMARKS IN BMPDFHESEG METHOD.

C^*	M_2^*	Notation
$C^*(w_{k_1}, w_{k_2}) = min(w_{k_1}, w_{k_2})$	$M_2^*(w_{k_1}, ..., w_{k_8}) = \frac{1}{7}\sum_{\substack{i,j=1 \\ j\neq i}}^{8} w_{k_j}$	F_1
$C^*(w_{k_1}, w_{k_2}) = w_{k_1} w_{k_2}$	$M_2^*(w_{k_1}, ..., w_{k_8}) = \frac{1}{7}\sum_{\substack{i,j=1 \\ j\neq i}}^{8} w_{k_j}$	F_2
$C^*(w_{k_1}, w_{k_2}) = h\Big(\frac{w_{k_1}^2 + w_{k_2}^2}{w_{k_1, w_{k_2}}}\Big)$	$M_2^*(w_{k_1}, ..., w_{k_8}) = \frac{1}{7}\sum_{\substack{i,j=1 \\ j\neq i}}^{8} w_{k_j}$	F_3
Maximum	$max(w_1, ..., w_8)$	F_4
Averaging	$\sum_{i=1}^{8} w_8/8$	F_5

Table 2S
EXPERIMENTAL PERFORMANCE OF DISTINCT VARIATIONS OF THE BONFERRONI MEAN TYPE PRE-AGGREGATION OPERATOR AND THE CLASSICAL AGGREGATION OPERATOR FOR BENCHMARKING.

Function	DRIVE				STARE				HRF			
	Accuracy	Sensitivity	Specificity	MCC	Accuracy	Sensitivity	Specificity	MCC	Accuracy	Sensitivity	Specificity	MCC
F_1	**0.954**	0.685	0.979	0.700	0.955	0.697	0.976	0.679	0.954	0.773	0.970	0.709
F_2	0.950	0.745	0.969	0.697	0.952	0.739	0.969	0.677	0.953	0.785	0.968	0.707
F_3	0.951	**0.763**	0.970	**0.702**	**0.955**	**0.764**	0.971	**0.691**	0.956	**0.791**	0.970	0.717
F_4	0.954	0.671	**0.981**	0.696	0.955	0.689	**0.977**	0.677	**0.957**	0.765	**0.974**	**0.719**
F_5	0.949	0.760	0.967	0.673	0.954	0.732	0.972	**0.682**	0.955	0.775	0.971	0.713

Table 3S
COMPARATIVE ANALYSIS BETWEEN THE RESPONSES OBTAINED THROUGH BMPDFHESEG METHOD WHEN UTILIZING A SINGLE COLOR CHANNEL (I^G_{Pred}) AND ALL COLOR CHANNEL INFORMATION (I^C_{Pred}) OVER CONSIDERED DATASETS.

Datasets	BMPDFHESeg (I^G_{Pred})				BMPDFHESeg (I^C_{Pred})			
	Accuracy	Sensitivity	Specificity	MCC	Accuracy	Sensitivity	Specificity	MCC
DRIVE	0.950	0.746	0.970	0.698	**0.951**	**0.763**	**0.970**	**0.702**
STARE	0.953	0.749	0.970	0.684	**0.955**	**0.764**	**0.971**	**0.691**
HRF	0.955	0.747	**0.975**	0.714	**0.956**	**0.791**	0.970	**0.717**

SUPPLEMENTARY REFERENCES

[1] O. Ronneberger, P. Fischer, and T. Brox, "U-Net: Convolutional networks for biomedical image segmentation," in *Medical Image Computing and Computer-Assisted Intervention–MICCAI 2015: 18th International Conference, Munich, Germany, October 5-9, 2015, Proceedings, Part III 18*. Springer, 2015, pp. 234–241.

[2] W. Ding, Y. Sun, J. Huang, H. Ju, C. Zhang, G. Yang, and C.-T. Lin, "RCAR-UNet: Retinal vessel segmentation network algorithm via novel rough attention mechanism," *Information Sciences*, vol. 657, p. 120007, 2024.

[3] Y. Liu, J. Shen, L. Yang, G. Bian, and H. Yu, "ResDO-UNet: A deep residual network for accurate retinal vessel segmentation from fundus images," *Biomedical Signal Processing and Control*, vol. 79, p. 104087, 2023.